Geomicrobiology Journal
Publication details, including instructions for authors and subscription information:
http://www.tandfonline.com/loi/ugmb20

Iron Uptake Kinetics and Magnetosome Formation by *Magnetospirillum gryphiswaldense* as a Function of pH, Temperature and Dissolved Iron Availability

Cristina Moisescu [a b], Steeve Bonneville [b], Sarah Staniland [c], Ioan Ardelean [a] & Liane G. Benning [b]

[a] Institute of Biology Bucharest, Centre of Microbiology, Bucharest, Romania

[b] School of Earth and Environment, University of Leeds, Leeds, United Kingdom

[c] School of Physics and Astronomy, University of Leeds, Leeds, United Kingdom

Available online: 19 Aug 2011

To cite this article: Cristina Moisescu, Steeve Bonneville, Sarah Staniland, Ioan Ardelean & Liane G. Benning (2011): Iron Uptake Kinetics and Magnetosome Formation by *Magnetospirillum gryphiswaldense* as a Function of pH, Temperature and Dissolved Iron Availability, Geomicrobiology Journal, 28:7, 590-600

To link to this article: http://dx.doi.org/10.1080/01490451.2011.594146

Geomicrobiology Journal, 28:590–600, 2011

ISSN: 0149-0451 print / 1521-0529 online
DOI: 10.1080/01490451.2011.594146

Taylor & Francis
Taylor & Francis Group

Iron Uptake Kinetics and Magnetosome Formation by *Magnetospirillum gryphiswaldense* as a Function of pH, Temperature and Dissolved Iron Availability

Cristina Moisescu,[1,2] Steeve Bonneville,[2] Sarah Staniland,[3] Ioan Ardelean,[1] and Liane G. Benning[2]

[1]*Institute of Biology Bucharest, Centre of Microbiology, Bucharest, Romania*
[2]*School of Earth and Environment, University of Leeds, Leeds, United Kingdom*
[3]*School of Physics and Astronomy, University of Leeds, Leeds, United Kingdom*

The dynamics of iron uptake and magnetosome formation by the magnetotactic bacteria (MTB) *Magnetospirillum gryphiswaldense* was investigated at a broad range of pH, temperature and iron availability to evaluate the role of MTB in the iron biogeochemical cycle. Except at pH 5.0, all incubations have shown significant bacterial growth. However, magnetosome formation was limited at pH 8.0 and 9.0 as well as at 4°C, 10°C and 35°C. At optimal conditions (i.e., pH 7 and 28°C), the uptake rates of dissolved Fe(III) as a function of initial Fe concentration can be described by a Michaelis-Menten-type kinetic model with a maximum iron uptake rate, V_{max}, of 11 × 10^{-12} μmoles cell^{-1} h^{-1} and an affinity constant, K_s of 26 μM Fe. High resolution imaging of magnetosomes synthesized at the different pH values, revealed a large range of morphologies and sizes, which illustrate the impact of environmental conditions on the formation of magnetite crystals by MTB.

Keywords magnetotactic bacteria, iron dynamics, biomineralization, magnetite characteristics

INTRODUCTION

Prokaryotes of both domains Bacteria and Archaea, can mediate the formation of numerous mineral phases. One of the most well characterized examples of biologically controlled mineralization is the formation of intracellular magnetic nanoparticles by magnetotactic bacteria (MTB). MTB are a very diverse group of prokaryotes (Abreu et al. 2007; Fassbinder et al. 1990; Keim et al. 2004; Li et al. 2007; Lins and Farina 2004; Moskowitz et al. 2008) which exhibit the ability to orient and migrate along the geomagnetic field lines of the Earth. This ability is based on unique nanosized organelles called magnetosomes, usually comprised of iron oxides (magnetite - Fe_3O_4) (Frankel et al. 1979) or iron sulfides (greigite - Fe_3S_4) (Posfai et al. 1998). For the synthesis of their magnetosomes, MTB require significant amounts of iron which sometimes may exceed 2% of their dry weight (Blakemore et al. 1979).

For these microorganisms, the role of iron extends far beyond that of a nutritional necessity, MTB having a remarkable potential to accumulate large amounts of iron, sometimes against a large concentration gradient, which suggests that they may play an important role in regulating parts of the iron cycle in sedimentary environments (Simmons and Edwards 2007; Simmons and Edwards 2006). Moreover, the biomineralization process performed by magnetotactic bacteria, may tie up iron in the form of magnetosomes thereby making a significant amount of iron unavailable for other organisms (Martins et al. 2007).

Although much attention has been focused upon the mechanisms of biomineralization in these microorganisms (Bazylinski et al. 1995; Mann et al. 1990; Schüler 2002; Stolz 1992; Taylor and Barry 2004), only limited information is available concerning the iron uptake dynamics by MTB (Schubbe et al. 2003; Schüler and Baeuerlein 1996, 1997, 1998). It is worth noting that although these studies were performed with the classical MTB, *Magnetospirillum gryphiswaldense* (strain DSM 6361) all were carried out with the MTB grown under optimum conditions (i.e. pH 7.0 and 28°C).

However, in nature, such constant conditions are unlikely to be found at all times, and MTBs could be found in waters at varying temperatures or pH values due to short-time (e.g., tidal sediments) or seasonal environmental variations. As the potential contribution of MTB to the biogeochemical iron cycling could be quantitatively significant (e.g., the total flux of iron contained in MTB minerals is 2 μg Fe cm^{-2} yr^{-1}) (Simmons and Edwards 2007), an estimation of their contribution to the biogeochemical iron cycle becomes also necessary. Faivre et al. (2008)

Received 6 August 2010; accepted 1 June 2011.
Address correspondence to Liane G. Benning, School of Earth and Environment, University of Leeds, Leeds LS2 9JT, UK. E-mail: l.g.benning@leeds.ac.uk

previously suggested that these three key-parameters (i.e., iron bioavailability, pH and T) may impact the physiology of the cells and consequently affect the physical and microstructural characteristics of the biogenic magnetite nanoparticles, yet an experimental evaluation is still lacking. Therefore, in the present study, we simulated variations in environmental parameters to quantify the dynamics of iron uptake by the same magnetotactic bacteria *Magnetospirillum gryphiswaldense* (strain DSM 6361) and evaluated the effect of these variations on magnetosome formation.

This was done as a function of iron bioavailability, solution pH, and growth temperature with a view to evaluate the possible contribution of magnetotactic bacteria to iron cycling and its export to sediments. Our study is thus the first to systematically describe the specific growth rates and iron kinetics for a range of iron concentrations, solution pHs, and temperatures, and to present a complete set of kinetic parameters (Fe uptake rates, affinity constant), crystal-size distributions, aspect ratios and morphologies for magnetite crystals synthesized by a MTB.

MATERIALS AND METHODS

Bacterial Strain and Growth Conditions

Magnetospirillum gryphiswaldense (strain DSM 6361, Schleifer et al. 1991; Schüler and Köhler 1992) was used as a model microorganism as it is a well-known microorganism for magnetite (Fe_3O_4) magnetosome production from dissolved Fe(III) (Schüler and Baeuerlein 1998). Cells were pre-grown to the mid-exponential phase under microaerobic conditions, without agitation, at pH 7.0 and 28°C, in a flask with standard medium, which contained (per liter deionized water): 0.1 g KH_2PO_4, 0.15 g $MgSO_4{\cdot}7H_2O$, 2.38 g Hepes, 0.34 g $NaNO_3$, 0.1 g yeast extract, 3 g soy bean peptone, 1 ml resazurin 0.5 g/L, and 1 ml EDTA chelated trace element mixture (Widdel and Bak 1992). In addition, the medium contained 27 mM sodium pyruvate as the sole carbon source. Iron was added before autoclaving as ferric citrate (100 μM added as ferric ammonium citrate; $NH_4Fe(C_6H_5O_7)$ and the pH of the medium was adjusted to 7.0 with NaOH (Heyen and Schüler 2003) supplemented with 100 μM). The culture flasks were filled to about 70% of their capacity, sealed with butyl-rubber stoppers and microaerobic conditions arose through the cellular oxygen (Schüler et al. 1998).

The cultures were sampled through the stopper with a hypodermic needle. Bacterial growth was monitored by measuring the optical density at 565 nm (OD_{565}) using an $UNIKON_{XL}$ spectrophotometer (Northstar Scientific Ltd.) and the culture magnetism was monitored qualitatively by placing the bacterial cultures on a magnetic stirrer and observing the rotation of the culture media in the direction of the rotating magnet.

The specific growth rate constant, μ (hours^{-1}), and the generation time, T (hours), the two parameters commonly used to define the growth of a bacterial population with regard to a given experimental condition were mathematically described using equations 1 and 2 (Maier et al. 2009):

$$\mu = \frac{dx}{xdt} \quad [1]$$

$$T = \frac{\ln_2}{\mu} \quad [2]$$

where x is the number or mass of cells (mass per unit of volume), and t is the time (h).

Determination of Cell Density and Biomass Dry Weight

The presence of magnetosome affects both the optical density and the total dry weight of the biomass. Therefore, in order to obtain cell density values, equivalent aliquots were used to determine both the OD_{565} and the cell counts (direct counting of propidium iodide stained-cells via epifluorescence microscopy) (Bonneville et al. 2006; Hobbie et al. 1977). For the biomass dry weight determinations, an equal volume of sample (i.e., bacterial culture possessing magnetosomes) was filtered through pre-weighed 0.2 μm polycarbonate filters (Millipore). After washing with ammonium acetate (20 mM) (Heyen and Schüler 2003), the filters were freeze-dried for 24 h and the dry weight determined gravimetrically. From this combined data, a calibration curve of OD_{565} and biomass dry weight for a culture possessing magnetosomes was constructed (data not shown).

Fe(III) Uptake Kinetic Studies

M. gryphiswaldense cells (cultured to the mid-exponential phase; Schüler et al. 1998) were re-suspended in fresh medium to initial cell densities of $\sim 2.3 \times 10^{10}$ cells L^{-1}. A first set of experiments was carried out with initial dissolved Fe(III) concentrations of 0, 4, 9, 12, 20, 30, 60 and 100 μM at a constant temperature (28 $\pm$ 0.5°C) and at pH 7.0. Equivalent experiments at pH 7.0, 28°C and with 100 μM Fe but with no bacteria were run as control. The effect of pH was evaluated at a constant temperature (28 $\pm$ 0.5°C) in the presence of 100 μM Fe(III). The pH was adjusted to 5.0, 6.0, 7.0, 8.0 and 9.0, using 0.1 M HCl or 1M NaOH.

In all experiments the Fe concentration in the fresh media was analyzed before and after filtration through 0.2 μm PVDF filters (Watman). The measurements revealed that the iron concentration did not vary, ensuring that no independent precipitation of Fe phases occurred in the media. Furthermore, samples from all experiments were imaged at high resolution (see below) and no particulate Fe phases outside the cells were observed. Finaly, for the temperature dependent experiments (4, 10, 20, 28, and 35 $\pm$ 0.5°C), the incubations were carried out at pH 7.0 with fresh medium containing 100 μM Fe(III). The experiments were carried out for up to three months in a static mode (i.e., no stirring, except before sampling when the bottles were rigorously shaken to ensure homogenization).

During the initial phase of the experiment, aliquots of the cell suspensions were sampled every 6 hours and monitored

for both bacterial growth (OD_{565}) and dissolved iron concentrations via the ferrozine method (Viollier et al 2000). For the dissolved iron measurements, the samples were filtered (in order to remove the cells) through 0.2 μm PVDF filters (Watman) directly into 0.5 M HCl. The Fe(III) uptake was monitored by quantifying the total Fe in the cell-free medium solution. The total amount of Fe(III) deposited intracellularly by the bacterial cells (as magnetosomes) was calculated from the difference between the initial and final iron concentration for each experiment.

The dependence of Fe(III) uptake rate on the extracellular Fe(III) availability was evaluated using the Michaelis-Menten kinetic model (Michaelis and Menten 1913). This model results in values for the uptake rate *v,* in μmol Fe(III) cell^{-1} hour^{-1}. This is done by linking v_{max}, the maximum specific Fe(III) uptake rate in μmol Fe(III) cell^{-1} hour^{-1} with the substrate iron concentration in μM, and the affinity constant for the substrate K_m also in μM.

High-Resolution Transmission Electron Microscopy (HR-TEM) and Image Analysis

M. gryphiswaldense cells were cultured via five consecutive incubations in iron-free culture media (to impair magnetosome synthesis, Faivre et al. 2008). These cells were subsequently grown at pH 5.0 to 9.0 in fresh culture media containing 100 μm Fe. Once the stationery phase was reached (evaluated from OD_{565}), the cells were harvested by centrifugation (13,000 rpm for 10 min) and washed twice with acetate buffer solution. Shortly before HR-TEM observations, one drop of a cell suspension was placed onto a holey carbon-coated Cu TEM grid (Agar Scientific Ltd., UK) and left to dry at room temperature. The magnetosomes were imaged with a FEI CM200 instrument equipped with a field-emission gun operated at an acceleration voltage of 200 kV using a Gatan Imaging Filter (GIF).

For statistical analysis of the sizes and shapes of the synthesized bacterial magnetites, at least 100 particles were measured in each sample (except pH 9.0 where only 34 particles were found). The crystal outlines in each cell were digitized and their dimensions calculated from the best fit of an ellipse to the contours of the crystals, with the ellipse having an area and dimensions less than or equal to those of the crystals (Devouard et al. 1998).

Image analyses were carried out using the software ImageJ (Abramoff et al. 2004; http://rsbweb.nih.gov/ij/). The shape factors for the magnetosomes were calculated from the measured crystal width to length ratios. The particle sizes (particle diameter) are reported as the average of length (L) and half-length width (W) of the measured ellipse (Devouard et al. 1998). For the average number of crystals per cell estimation, between 10 and 15 cells were counted. Statistical analysis was performed using standard statistical methods.

RESULTS

Effect of Iron Availability on Bacterial Growth and Iron Uptake Kinetics

As shown in Figure 1a, the fast increase in biomass in the first 24 h was mirrored by a sharp decrease in dissolved iron concentrations; this correlation was observed for all initial dissolved Fe(III) concentrations tested. Once the bacterial cultures reached the stationary phase and thus only a slight increase in biomass is further observed over time, the iron uptake also slowed down.

Applying equations 1 and 2 to the data from the bacterial growth curves at all conditions tested, yielded values for the specific growth rates (i.e., μ in h^{-1}), and generation times (T, in h) in all experiments (Table 1).

Interestingly, only a small increase in the specific growth rate and a concomitant decrease of the generation time was observed with increasing initial Fe concentration (Figure 1b). In the experiments with no added Fe(III), the bacteria however also grew, but this growth was solely supported by trace amounts of residual iron (i.e., 0.2 μM) in the culture media. Therefore, initial Fe(III) availability was not limiting the growth of the bacteria. In contrast to the cultures amended with Fe(III), the initial weak magnetism in the non-Fe amended experiments decreased progressively as growth proceeded.

For the Fe(III) uptake experiments, in which the initial dissolved Fe(III) varied from 0 to 100 μM, the Fe(III) uptake rates (μmol h^{-1} cell^{-1}) were derived from a linear regression of the Fe(III) concentrations over time during the exponential growth phase (Figure 1a). The data are plotted in Figure 1c against initial dissolved Fe(III). This way we could evaluate the link between the Fe(III) uptake rates, magnetosome formation and the availability of iron in the system (Figure 1c). When the cells were grown in the presence of various initial dissolved Fe(III) concentrations, the uptake rates exhibited saturation-type kinetics with increasing Fe(III) availability (Figure 1c).

Using the non-linear fitting procedure in the Michaelis-Menten model, the best-fit values of v_{max} and K_m derived from the experimental data were 11 $\pm$ 1.6 μmol h^{-1} cell^{-1} (i.e., 0.8 $\pm$ 0.1 nmoles min^{-1} (mg dry weight)$^{-1}$), and 26.7 $\pm$ 9.3 μM Fe(III), respectively. Three previous studies that also used *M. gryphiswaldense* cultures, reported values for v_{max} (Faivre et al. 2008; Schubbe et al. 2003; Schuler and Baeuerlein 1996), which are in good agreement with our values (i.e., 1, 0.46, and 0.86 respectively, nmoles min^{-1} (mg dry weight)$^{-1}$). However, compared to the previously reported values (i.e., 21.6 and 3, respectively, μM Fe(III)) (Schubbe et al. 2003; Schuler and Baeuerlein 1996), our K_m, was up to 9 times higher (26.7 $\pm$ 9.3 μM Fe(III)) (Table 2).

In Schuler and Baeuerlein (1996), a Lineweaver-Burk plot was used to estimate the v_{max} and K_m values. When applied to our data set (Figure 1d), we obtained a v_{max} value of 13.0 $\pm$ 7.8 μmol h^{-1} cell^{-1} (i.e., 0.9 $\pm$ 0.5 nmol min^{-1} per mg dry weight) and a K_m value of 35.5 $\pm$ 23.3 μM Fe(III). These are

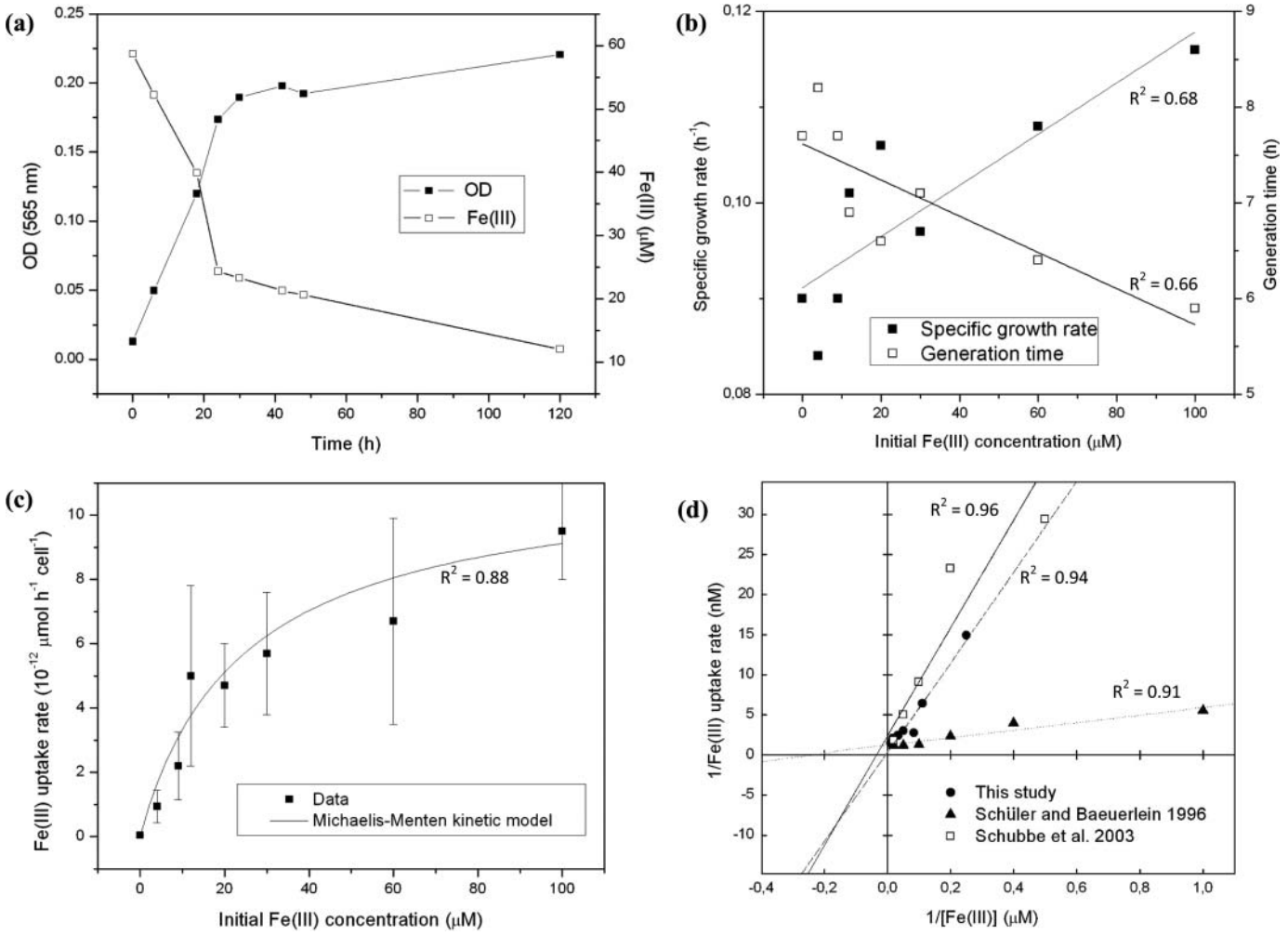

FIG. 1. Growth and iron uptake dynamics of *M. gryphiswaldense* cells. All data from experiments at 28°C, and pH 7.0. (a) optical density and iron uptake cells grown at 60 μM extracellular Fe(III). (b) Specific growth rate and generation time as a function of initial dissolved Fe(III) concentration. Note the difference in the two Y axes. (c) Michaelis-Menten plot of the Fe(III) uptake rates at different initial dissolved Fe(III) concentrations with errors bars indicating the standard deviation of the slope of the linear least squares regression of the total Fe(III) uptake. The following apparent kinetic constants were calculated: $K_m = 26.7 \pm 9.3$ μM Fe(III) and $v_{max} = 11 \pm 1.6$ μmol h^{-1} cell^{-1}. (d) Lineweaver-Burk plot of the Fe(III) uptake rates at different initial dissolved Fe(III) concentrations. The apparent kinetic constants calculated from the Lineweaver-Burk plot were: $K_m = 35.5 \pm 23.3$ μM Fe(III) and $v_{max} = 13.0 \pm 7.8$ μmol h^{-1} cell^{-1}.

in line with our previous values calculated using the non-linear fit, yet with much larger errors.

Effect of Solution pH and Temperature on Growth and Fe(III) Uptake Kinetics

In our experiments, dissolved iron uptake and bacterial growth rates were monitored for a large range of temperatures (4–35°C) and pH (5.0 to 9.0) in order to evaluate how these key-parameters might affect the biomineralization process of magnetosomes and the development of MTB cultures. The optimum conditions for the used *M. gryphiswaldense* strain were pH 7.0 and 28°C (Figures 2 and 3). These are in agreement with the optimum cultivation conditions for other known magnetotactic bacteria (Arakaki et al. 2003; Blakemore 1975; Blakemore et al. 1979; Heyen and Schüler 2003).

The optimal pH for growth was at pH 7.0, yet significant growth, high levels of iron uptake as well as variable magnetosome formation were observed at all tested pH regimes except at pH 5.0, where neither growth nor magnetosome formation were detected (Table 1, Figures 2 and 3). Excluding the optimum condition at pH 7.0 and the lethal pH 5.0, a clear decrease in growth rates at pH 6.0, 8.0, and 9.0 was observed. Compared to pH 7.0, the iron uptake rate was reduced by a factor of 4 up to 17 and the following trend was observed: pH 8.0 > pH 6.0 > pH 9.0 (Figures 2 and 3).

In support of these data are the results from the actual TEM observations of magnetosome abundance at the tested conditions where the images showed a direct correlation between the Fe(III) uptake rate and the average number of magnetosomes per cell (Table 3). The only deviation from the linearity was

TABLE 1
Influence of extracellular Fe concentrations, solution pH, and temperature on growth rates, generation times, and iron uptake dynamics of *M. gryphiswaldense* cells

	Specific growth rate (h^{-1})	Generation time (h)	Fe uptake rate (10^{-12} μmol h^{-1} $cell^{-1}$)	Intracellular Fe (10^{-11} μmol $cell^{-1}$)
[Fe] (μM)				
0	0.090	7.7	0.0	0.0
4	0.084	8.2	0.9	1.4
9	0.090	7.7	2.2	3.3
12	0.101	6.9	5.0	4.1
20	0.106	6.6	4.7	6.2
30	0.097	7.1	5.7	11.1
60	0.108	6.4	6.7	13.2
100	0.116	5.9	9.5	16.9
pH				
5	0.001*	468.5*	0.0	0.0
6	0.016	42.6	1.02	6.1
7	0.099	7.0	6.8	16.1
8	0.045	15.6	1.7	13.3
9	0.018	26.4	0.4	3.8
T (°C)				
4	0.002	135.8	0.01	1.2
10	0.013	55.2	1.1	5.5
20	0.041	27.7	1.7	10.8
28	0.099	7.0	6.8	16.1
35	0.004	196.7	0.06	3.2

*Specific death rate (Maier, Pepper et al. 2009).

observed at pH 6.0, where the average number of magnetosomes per cell did not reflect the smaller Fe(III) uptake rate. This difference can be explained by the variations in average diameters of the synthesized magnetosome particles (Table 3 and Figure 4). At the optimum pH (i.e., pH 7.0), the synthesized magnetites had an average diameter of 46 ± 7 nm, at pH 6.0 the particles were approximately half in size (29 ± 12.3 nm), and at pH 8.0 and 9.0 they were similar in size (47 ± 12 nm and 45 ± 10 nm) but the standards deviation at this non-optimal pH values were larger (Table 3 and Figure 4).

Within the range of temperature considered, when compared with the optimal conditions at 28°C, very large variations in terms of culture growth and iron uptake were measured (Figure 2). The growth rate and iron uptake rate decreased as follows: 20°C > 10°C > 35°C > 4°C. Similar to the pH effect described here, when the temperature-dependent rates were compared to the optimal temperature (28°C), the rates measured at 20°C and 10°C were slower by a factor of 4 and 6 respectively. They were even slower at 35°C and 4°C. At 4°C, even though a noticeable Fe(III) uptake rate was measured, we were unable to detect any magnetosome particles inside the cells when imaged by TEM. Overall, it is noteworthyto mention that irrespective of the large temperature and pH induced variations in Fe uptake rates (>1 order of magnitude), the average diameter of the formed

TABLE 2
Comparison between the v_{max} and K_m values obtained from the present work and previously reported studies

	v_{max} (nmoles min^{-1} (mg dry weight)$^{-1}$)	K_m (μM)	Reference
Michaelis-Menten	0.8 ± 0.1	26.7 ± 9.3	This work
	1	N.A.	Faivre et al. 2008
	0.46	21.6	Schubbe et al. 2003
Lineweaver-Burk	0.9 ± 0.5	35.5 ± 23.3	This work
	0.86	3	Schüler and Baeuerlein 1996

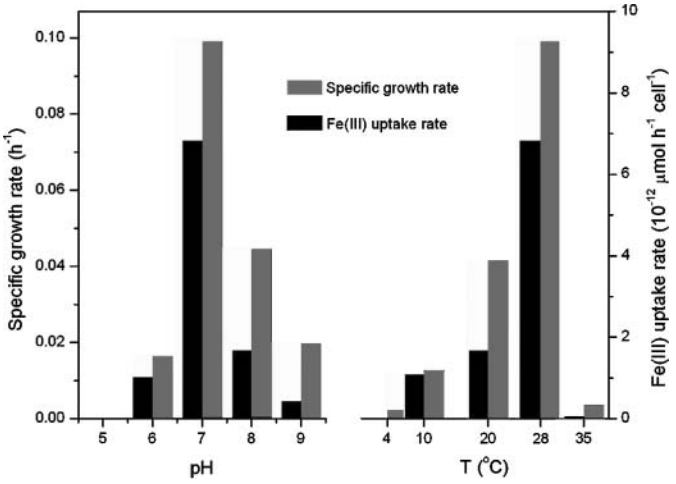

FIG. 2. Specific growth rates (left y-axis) and kinetics of iron uptake (right y-axis) by *M. gryphiswaldense* at 100 μM added iron, temperature of 28°C, and at different pH values (left side of the plot), and 100 μM added iron, pH 7.0 and different temperatures (right side of the plot).

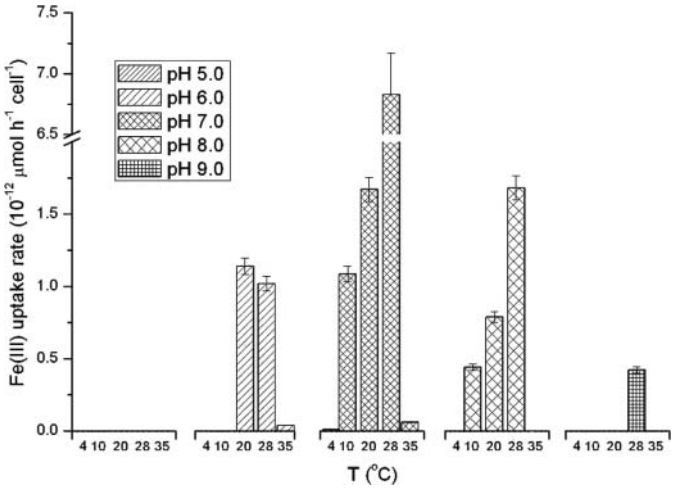

FIG. 3. The combined effect of pH and temperature variation on the iron uptake dynamics in *M. gryphiswaldense* cells.

magnetosomes all lay in an extremely narrow size range (i.e., 43 to 47 nm on average—Table 3).

Finally, it is noteworthy that regardless of the tested variations in experimental conditions (i.e., initial Fe(III) concentration, pH or temperature), a clear positive correlation between the specific growth rate and the Fe(III) uptake rate was observed (Figure 2).

Ultrastructural Characteristics of the Synthesized Magnetite Crystals

In a previous study (Moisescu et al. 2008), we showed that the crystals grown at neutral pH and 28°C exhibited roughly equidimensional cuboctahedral morphologies, with a narrow crystal size distribution (46 $\pm$ 6.8 nm), high crystallinity (single domain crystals) and high chemical purity. In the present study, the sizes and morphologies of the crystals synthesized at 10°C and 20°C (no crystals were found at 4°C and 35°C) were similar to the crystals formed under optimum conditions. Essentially, this shows that MTBs are able to preserve their abilities to control the biomineralization process between 10°C and 28°C despite a clear decrease in the number of magnetosomes formed (Table 3).

Due to the lack of data on the temperature effect on magnetosome characteristics, we focused our ultrastructural study on the crystals synthesized by cells grown at 28°C for different pH values. Compared with the magnetite particles formed under optimal pH conditions (pH = 7), the crystals formed in cells grown at pH 6.0, 8.0 and 9.0 revealed a different behavior. We observed a wider size distribution (Figure 4b), the presence of many crystal defects (Figure 4a) and even completely different morphologies (Figure 4a).

The crystals formed at pH 6.0 showed poor crystallinity (Figure 4a), broad crystal size distributions (CSD) and shape-factors (SFD) (Figure 4b, 4c), as well as the lack of a specific crystal morphology. As a result, the majority of the pH 6.0 magnetite crystals fell outside the single-domain field (35–120 nm) but

TABLE 3
Statistical data for magnetosomes synthesized by *M. gryphiswaldense* at l00 μM iron, at different pH values and different temperatures

	pH					T°C				
	5.0	6.0	7.0	8.0	9.0	4	10	20	28	35
Average number of crystals per bacterium	0	15	39	11	3	0	10	28	39	0
Average diameter (nm $\pm$ SD)	N.D.	29 $\pm$ 12.3	46 $\pm$ 6.8	47 $\pm$ 12	45$\pm$ 10.3	N.D.	43 $\pm$ 9.8	45 $\pm$ 13.6	46 $\pm$ 6.8	N.D.

For pH 9.0 we only considered the cuboctahedral crystals and excluded the triangular ones shown in Fig. 4a right-hand image, white arrow; (SD, 1σ Standard Deviation; N.D. not determined).

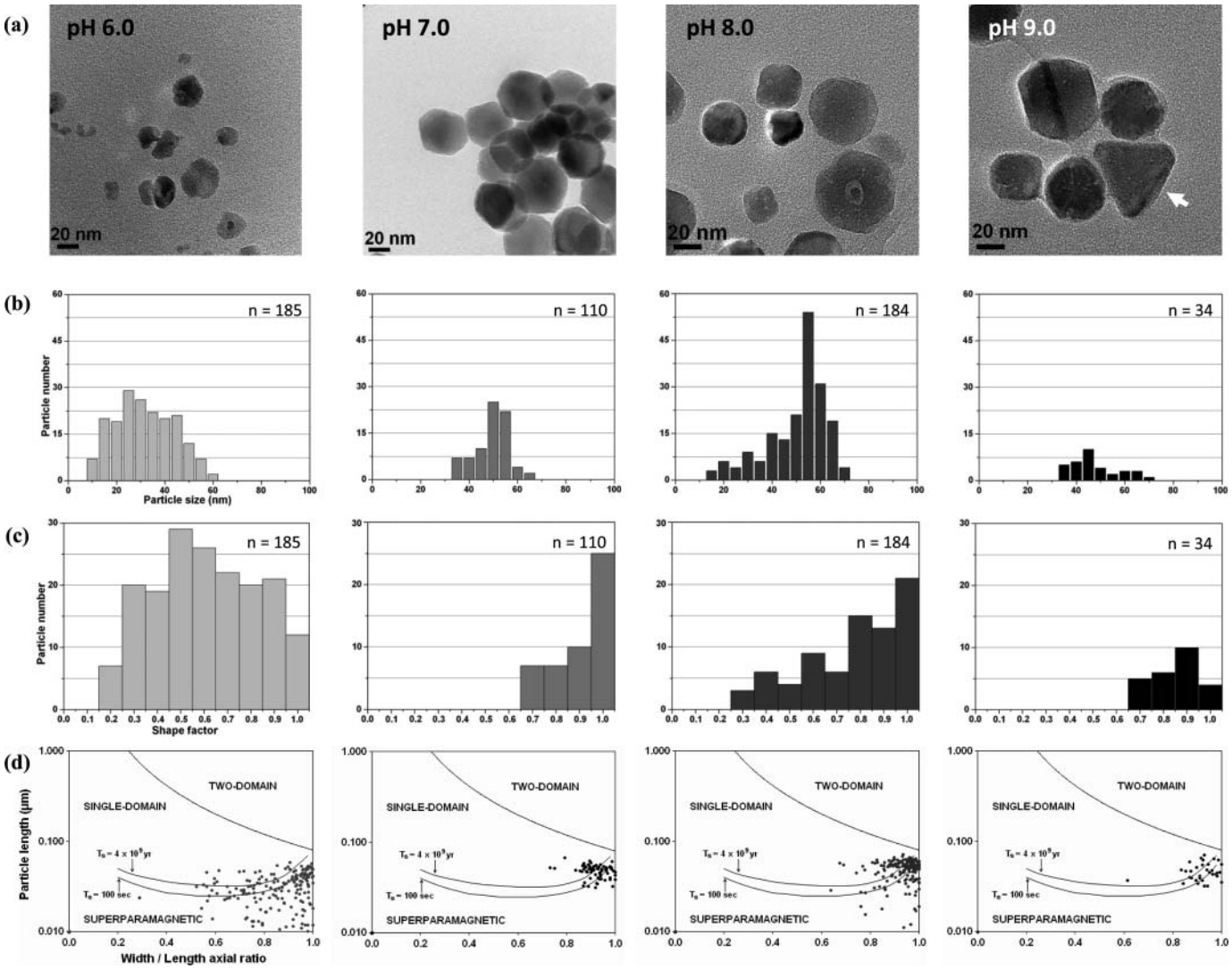

FIG. 4. (a) TEM images, (b) crystal size distributions (CSDs), (c) shape factor distributions (SFDs), and (d) CSDs plotted on a Butler-Banerjee diagram of magnetite crystals synthesized by *M. gryphiswaldense* cells grown with 100 μM, at 28°C and at different pH values. Boundaries between magnetic single-domain and superparamagnetic stability fields were drawn according to Butler and Banerjee (1975).

in the superparamagnetic region (Figure 4d) (Moskowitz 1995). The CSD of these crystals (Figure 4b at left) have a normal asymmetric distribution, with a sharp cut-off towards smaller sizes, a positive skewness of 0.16, and a shape factor <0.75 (Figure 4c at left). These are typical characteristics of immature magnetosomes (Faivre et al. 2008) or inorganic synthetic magnetite nanocrystals (Devouard et al. 1998; Faivre and Zuddas 2006).

A similar trend was observed at pH 9.0 (Figure 4 right-most column). Here the crystals are characterized by a variety of sizes and shapes, culminating with prismatic crystal (Figure 4a, left upper image, white arrow). Compared to the pH 6.0 crystals, the magnetosomes formed at pH 9.0 are well-defined and noticeably bigger with the majority falling within or at the very margin of the single-domain field (Figure 4d). Thy also have a 0.6 positively skewed CSD, and a narrow SFD with a distinct maximum at 0.9. In contrast, at pH 8.0 the magnetosomes were characterized by slightly larger crystals (i.e., 47 nm on average—Table 1), round morphologies, negatively skewed CSD (i.e., −1.5), and asymmetric SFD with a maxima equal to 1, corresponding to isometric shape crystals.

Overall, our results showed that the majority of the particles meet the requirements for single-domain behavior (Butler and Banerjee 1975; Diaz-Ricci and Kirschvink 1992), falling within the single-domain range (Figure 4d). Smaller particles (20–30 nm) fell outside the single-domain field, and within the superparamagnetic region. Similarly, the perfectly isometric particles with an axial ratio of ∼1.0 plotted at the very margin of the single-domain field and in the superparamagnetic region. It is important to note that no mineral phases other than magnetite were detected in our experiments.

DISCUSSION

The results suggests that the iron requirement of the magnetotactic bacteria cultures is much higher during the exponential growth phase when the cells are actively dividing and synthesizing new magnetosome chains (Staniland et al. 2010). In addition, the dissolved Fe(III) is deposited almost immediately as magnetite inside the magnetosome vesicles (Schüler and Baeuerlein 1998; Staniland et al. 2007).

In contrast to their capacity to accumulate large amounts of iron, the ability to grow at low to very low dissolved iron concentrations also suggests that iron is a limiting factor only for magnetite formation inside the magnetosome vesicles. However, the presence of iron is not a limiting substrate for the growth of the MTB themselves. This observation is in agreement with previous TEM investigations of magnetotactic cells grown in the absence of added iron (Schüler and Baeuerlein 1996), who reported the presence of only a few immature crystals coupled with a decrease in the culture magnetism.

A limited number of studies quantifying iron uptake kinetic parameters are available for magnetotactic bacteria, making a comparison difficult. However, our resuls confirm and support the few previously published papers in terms of v_{max} and K_m, with the only discrepancy being the K_m value. One possibility for this discrepancy is the Lineweaver-Burk calculation method, which is prone to generate large errors because the linear regressions are skewed heavily towards experiments performed at very low initial substrate concentrations where inherent experimental uncertainties are maximal.

However, we believe that the difference between the K_m value in the present study and Schüler and Baeuerlein's (1996) K_m value (Table 2) is not due to calculation method but rather due to the differences in experimental conditions and/or medium composition. Indeed, in Schüler and Baeuerlein (1996), the cells used as inoculum had been previously grown in iron depleted conditions and as a consequence cells exhibiting a high affinity for iron were pre-selected. Therefore, once exposed to high dissolved Fe(III), those cultures showed a lower K_m than measured in our experiments, where the cells originates from a culture with 100 μM of dissolved Fe(III).

This observation emphasizes the influence of the inoculum preparation and growth medium composition on the overall ability of the MTB to interact with dissolved iron. Nevertheless, our K_m value derived using the Michaelis-Menten approach (26.7 ± 9.3 μM Fe(III)) is comparable to the 21.6 μM Fe(III) value for K_m reported by Schubbe et al. (2003). Those authors suggested the presence of a low-affinity transport system in *M. gryphiswaldense* cells in accordance with the absence of siderophore-like compounds in MTB (Nakamura et al. 1995; Schüler and Baeuerlein 1996), which is thought to exhibit a very high-affinity towards dissolved iron (Winkelmann 1991).

Interestingly, our K_m value is approximately half that of the K_m value reported for the Fe(III) reductase enzyme purified from *Magnetospirillum gryphiswaldense* MSR-1 strain grown in the presence of the aqueous complex of Fe-citrate (Xia et al. 2007). This Fe reductase enzyme is involved in the first step of magnetosome formation, i.e., the active uptake of Fe(III) via a reduction step (Schüler 1999). Therefore, the high values of the calculated K_m in our experiment could be due to the activity of this enzyme.

The final question we addressed was if and how the pH and temperature variations affected the ultrastructure of the magnetite crystals produced by MTB. Indeed, other studies have shown that changes in growth conditions such as the presence of other dissolved chemical species, pH, redox potential (Eh), ionic strength, temperature, and pressure can influence the size distribution and habit of the bio-synthesized crystals (Bazylinski and Frankel 2004; Faivre et al. 2008). Magnetite crystals formed by magnetotactic bacteria at optimal growth conditions are usually characterized by high chemical purity, narrow size ranges, species-specific crystal morphologies and they exhibit specific arrangements within the cell (e.g., Moisescu et al. 2008; Schüler 1999).

These features indicate that the formation of magnetosomes is happening under precise biological control (Bazylinski and Frankel 2004). It is also possible, however, that the role of the MTB is limited to providing a suitable 'constraint' chemical environment (e.g., specific pH, Eh, ionic strength etc.) favorable for precipitation of magnetite (Schüler and Baeuerlein 1998). If so, changes in the environmental conditions of the bulk culture solution may interfere with the formation of magnetite inside the magnetosome vesicles (Faivre et al. 2008). Yet, little is known about these effects.

According to Faivre et al. (2008), slower iron uptake rates (as observed in the current study at pH 6.0, 8.0, and 9.0) induce a more controlled biomineralization process and therefore the formation of magnetosomes with better-defined sizes and shapes. Surprisingly, this was not the case in our study. Indeed, the cells grown at pH 6.0 exhibited an iron uptake rate approximately 6–7 times slower than under optimal conditions.

Interestingly however, the corresponding magnetite crystals resembled more immature or poorly developed crystals (Faivre et al. 2008) or extra-cellular minerals formed by biologically induced mineralization (BIM) (Bazylinski et al. 2007; Frankel and Bazylinski 2003) a process that forms very different magnetite than those produced via biologically controlled mineralization (BCM).

Overall, our results suggests that not only the iron uptake rate is influencing the size and morphology of the crystals as previously showed by Faivre et al. (2003) but also other environmental parameters and especially pH have a great impact on the number, sizes and morphologies of the bacterial magnetite crystals (Table 1 and Figures 2 and 3). Interestingly, the tested temperature variations induced either a total inhibition of magnetosome formation (incubation at 4°C and 35°C) or no change in the magnetite crystal morphologies and dimensions (incubation at 10°C and 20°C, Table 3).

The latter aspect is surprising as the Fe uptake rate decreased substantially away from the optimum 28°C. This implies that between 10°C and 28°C the crystals characteristics are not directly linked to the Fe uptake rate and that the bacteria are able to cope with the temperature change. However, outside this range (i.e., <10°C and >35°C) and at non-neutral pH, the intracellular metabolism and chemistry is highly affected by the surrounding chemical conditions (pH and temperature values) and the cells are unable to control the magnetite biomineralization process.

Under those stress conditions, although the MTB still grow and produce magnetosomes, the cells tend to concentrate on vital functions and on preserving their cell integrity. Indeed, under optimum conditions, membrane bound proteins are governing the crystal morphology (Matsunaga and Sakaguchi 2000; Nakamura et al. 1995; Okamura et al. 2001). However, under less favorable conditions, the synthesis of the necessary proteins for magnetosome synthesis may be quantitatively reduced or even stopped. Therefore, in our experiments, the variations in the shapes and morphology of the magnetosomes formed at various pH conditions (Figure 4) may primarily be the result of spontaneous magnetite precipitation rather than controlled by the bacteria themselves. That is why, even in the case of a slow synthesis (as opposed to fast growing magnetosomes, Faivre et al. 2008) the magnetosome size and especially morphology will be affected. In addition, although the optimal conditions of this MTB strain growth is at 28°C and pH 7.0, our data clearly indicates that this strain is able to also easily grow at other temperatures (e.g., at 10–20°C), which are more representative of natural conditions. However, non-neutral pH conditions have a strong effect on the crystals shape, morphology and size distribution (Figure 4).

An important implication of these environmental effects on the size and morphology of the biogenic magnetite is linked to the assessment of the origin of magnetic nanoparticles in sediments. Indeed, their provenance is often evaluated using the size and morphology of the crystals. For instance, a special case is the magnetite crystals found in the Martian meteorite ALH84001. Based on their resemblance with the magnetosomes of terrestrial MTB's the se crystals were suggested to possibly represent magnetofossil remnants (Friedmann et al. 2001; Thomas-Keprta et al. 2000, 2001).

Thus, the results of the present study showed that the pH of the growth solution greatly affects the size and shape of the biogenic magnetite crystals, making them in some cases similar or equivalent in size and shape to inorganically produced magnetite particles. This suggests that the morphology and crystal characteristics alone should not be used as sole criteria in establishing the biotic or abiotic origin of magnetite nanoparticles.

Potential Contribution of MTB to the Biogeochemical Cycling of Iron

Based on our current and published data (Simmons and Edwards 2007), the contribution of MTB to the biogeochemical iron cycle, can be estimated using the following set of parameters: cell density, Fe content per cell, chemocline width, and population turnover times (i.e., generation time). Considering that the present study was performed under laboratory conditions, in batch cultures with moderate agitation due to the periodic sampling which prevented the formation of any type of cline (i.e., chemocline, thermocline). Therefore, the chemocline width was excluded from the formula (Simmons and Edwards 2007), resulting in the following expression:

$$(\text{MTB density cells mL}^{-1}) \times (\text{intracellular Fe } \mu\text{moles or mg cell}^{-1}) \times (\text{MTB populations year}^{-1})$$

This allowed us to estimate roughly the amount of iron that could be extracted by a MTB population from a given volume of solution per unit of time (μmoles or mg Fe L^{-1} $year^{-1}$). To carry out this calculation we are taking into consideration that the approximate abundance of MTB in natural environments was reported to be around $\sim 10^5$ cells mL^{-1} (Bazylinski et al. 1995; Blakemore 1982; Simmons and Edwards 2007; Simmons et al. 2007) and the extracellular iron concentration in the natural habitat of MTB, was reported to be around 20 μM (Blakemore et al. 1979; Schüler 1994). Thus, we have calculated an Fe content of approximately 6×10^{-11} μmoles Fe $cell^{-1}$ (3×10^{-12} mg Fe $cell^{-1}$—Table 1) for *M. gryphiswaldense* cells grown at pH 7.0, 28°C in the presence of 20 μM added Fe(III).

Considering that the generation time for these cells varied between 6 and 197 h (Table 1) depending on the iron concentration, temperature or pH conditions, we estimated an average generation time of 34 h, and thus a population turnover of approximately 260 generations $year^{-1}$. At these conditions the contribution of MTB to the biogeochemical iron cycle is thus 1.6 μmoles Fe L^{-1} $year^{-1}$. This equates to approximately 0.078 mg Fe L^{-1} $year^{-1}$ iron tied up in a mineral form that is unavailable for other organisms (Barbeau et al. 1996).

Assuming that the dissolved Fe(III) concentration is constant and sufficient for unlimited growth and magnetite formation (i.e., 100 μM added iron), that the temperature is close to the optimum 28°C, and that the only fluctuating parameter is pH (between 5.0 and 9.0), we calculated that the quantity of iron accumulated by the MTB cells can reach between 3.8 and 16.1×10^{-11} μmol Fe $cell^{-1}$ (at pH 9.0 and 7.0, respectively). At these conditions, we estimate a potential pH-dependent contribution of MTB to the biogeochemical iron cycle of approximately 0.98 to 4.2 μmoles Fe L^{-1} $year^{-1}$, respectively, 0.06 to 0.24 mg Fe L^{-1} $year^{-1}$.

Similarly, if we assume that the iron concentration and pH value remain constant, and only the temperature is undergoing variations, we can estimate a temperature-dependent contribution of MTB to the biogeochemical iron cycle, of approximately 0.3 to 4.2 μmoles Fe L^{-1} $year^{-1}$ respectively 0.02 to 0.24 mg Fe L^{-1} $year^{-1}$.

CONCLUSIONS

The present study showed for the first time, the effect of environmental boundary conditions on the growth of *M. gryphiswaldense* and on the occurrence of magnetosomes in natural environments. Furthermore, we now have optimum laboratory cultivation conditions to compare with the natural observations. We showed that the iron supply in *M. gryphiswaldense* cultures even at adverse pH and temperature conditions is not limiting for cell growth but it is crucial for magnetite formation. However, the ideal conditions for growth and magnetosome formation are limited to a narrow range of dissolved iron concentrations, which are not often found in natural environments except in ferruginous basins like Lake Matano (Crowe et al. 2011).

At optimum conditions (pH 7.0 and 28°C), iron uptake is a relatively rapid process with a v_{max} of 11 μmol h^{-1} $cell^{-1}$ (i.e., 0.8 nmoles min^{-1} (mg dry weight)$^{-1}$) as compared with other known microorganisms. The kinetics can be described by a Michaelis-Menten model and although v_{max} can be considered a stable characteristic, as the derived value is the same order of magnitude in three independent studies, the K_m value can vary significantly depending on the experimental medium composition and the adaptation of the inoculum to scavenge dissolved Fe(III).

Not surprisingly, temperature and especially pH conditions are affecting the viability and the physiology of MTB and consequently their ability to control the magnetite biomineralization. Although growth occurred at almost all conditions tested (except at pH 5.0), large variations were observed in the resulting magnetosome sizes and morphologies. The size and the morphology of the magnetite crystals formed by *M. gryphiswaldense* cells at pH 6.0 and 8.0 are similar to abiotically precipitated minerals, while the prismatic magnetites formed at pH 9.0 are unique and have so far never been reported, in any other biological or non-biological system.

Finally, although we provide with this study a new wealth of data about magnetosome formation in MBT's, it is also clear that the unequivocal interpretation of the origin of magnetite crystals in natural samples (i.e., biogenic or abiogenic) is more complex than so far assumed. Therefore, when analyzing magnetite characteristics for their biogenicity, more care has to be taken in the evaluation as various environmental factors affect the size, shape or purity of biogenic magnetites and thus a distinction from inorganic magnetites is not straightforward.

ACKNOWLEDGMENTS

Thanks are due to the FP6 Marie Curie MIR-EST "Mineral-Fluid Interface Reactivity" Early Stage Training Network (MEST-CT-2005-021120) and the UK NERC "Weathering Science Consortium" (NE/C004566/1) for financially supporting the work. We also like to acknowledge LEMAS (the Leeds Electron Microscopy and Spectroscopy Center) for granting access to the electron microscopy and analysis facilities. Finally, we would like to acknowledge two anonymous reviewers whose contributions have greatly improved the manuscript.

REFERENCES

Abramoff MD, Magalhaes PJ, Ram SJ. 2004. Image processing with Image J. Biophotonics International 11:36–42.

Abreu F, Martins JL, Souza Silveira T, Keim CN, Lins de Barros HGP, Filho FJG, Lins U. 2007. 'Candidatus magnetoglobus multicellularis,' a multicellular, magnetotactic prokaryote from a hypersaline environment. Int J Syst Evol Microbiol 57:1318–1322.

Arakaki A, Webb J, Matsunaga T. 2003. A Novel protein tightly bound to bacterial magnetic particles in Magnetospirillum magneticum strain AMB-1. J Biol Chem 278:8745–8750.

Baeuerlein E. 2003. Biomineralization of unicellular organisms: An unusual membrane biochemistry for the production of inorganic nano- and microstructures. Angewandte Chemie - International Edition 42:614–641.

Barbeau K, Moffett JW, Caron DA, Croot PL, Erdner DL. 1996. Role of protozoan grazing in relieving iron limitation of phytoplankton. Nature 380:61–64.

Bazylinski DA, Frankel RB. 2004. Magnetosome formation in prokaryotes. Nature Rev Microbiol 2:217–230.

Bazylinski DA, Frankel RB, Heywood BR, Mann S, King JW, Donaghay PL, Hanson AK. 1995. Controlled biomineralization of magnetite (Fe_3O_4) and greigite (Fe_3S_4) in a magnetotactic bacterium. Appl Environ Microbiol 61:3232–3239.

Bazylinski DA, Frankel RB, Konhauser KO. 2007. Modes of biomineralization of magnetite by microbes. Geomicrobiol J 24:465–475.

Blakemore R. 1975. Magnetotactic bacteria. Science 190:377–379.

Blakemore RP. 1982. Magnetotactic bacteria. Annu. Rev. Microbiol 36:217–238.

Blakemore RP, Maratea D, Wolfe RS. 1979. Isolation and pure culture of a freshwater magnetic spirillum in chemically defined medium. J. Bacteriol 140:720–729.

Bonneville S, Behrends T, Cappellen PV, Hyacinthe C, Roling WFM. 2006. Reduction of Fe(III) colloids by Shewanella putrefaciens: A kinetic model. Geochim Cosmochim Acta 70:5842–5854.

Butler RF, Banerjee SK. 1975. Theoretical single-domain grain size range in magnetite and titanomagnetite. J Geophys Res 80:4049–4058.

Crowe SA, Katsev S, Leslie K, Sturm A, Magen C, Nomosatryo S, Pack MA, Kessler JD, Reeburgh WS, Roberts JA, Gonzalez J, Haffner GD, Mucci A, Sundby B, Fowle DA. 2011. The methane cycle in ferruginous Lake Matano. Geobiology 9:61–78.

Devouard B, Posfai M, Hua X, Bazylinski DA, Frankel RB, Buseck PR. 1998. Magnetite from magnetotactic bacteria: Size distributions and twinning. Amer Mineral 83:1387–1398.

Diaz-Ricci JC, Kirschvink JL. 1992. Magnetic domain state and coercivity predictions for biogenic greigite (Fe_3S_4): Comparison of theory with magnetosome observations. J Geophys Res 97:17309–17315.

Faivre D, Menguy N, Posfai M, Schüler D. 2008. Environmental parameters affect the physical properties of fast-growing magnetosomes. Amer Mineral 93:463–469.

Faivre D, Zuddas P. 2006. An integrated approach for determining the origin of magnetite nanoparticles. Earth Planet Sci Lett 243:53–60.

Fassbinder JWE, Stanjek H, Vali H. 1990. Occurrence of magnetic bacteria in soil. Nature 343:161–163.

Frankel RB, Bazylinski DA. 2003. Biologically induced mineralization by bacteria. Rev Mineral Geochem 54:95–114.

Frankel RB, Blakemore RP, Wolfe RS. 1979. Magnetite in freshwater magnetotactic bacteria. Science 203:1355–1356.

Friedmann EI, Wierzchos J, Ascaso C, Winklhofer M. 2001. Chains of magnetite crystals in the meteorite ALH84001: Evidence of biological origin. Proc Natl Acad Sci USA 98:2176–2181.

Heyen U, Schüler D. 2003. Growth and magnetosome formation by microaerophilic Magnetospirillum strains in an oxygen-controlled fermentor. Appl Microbiol Biotechnol 61:536–544.

Hobbie JE, Daley RJ, Jasper S. 1977. Use of nuclepore filters for counting bacteria by fluorescence microscopy. Appl Environ Microbiol 33:1225–1228.

Keim CN, Abreu F, Lins U, De Barros HL, Farina M. 2004. Cell organization and ultrastructure of a magnetotactic multicellular organism. J Struct Biol 145:254–262.

Komeili A, Li Z, Newman DK, Jensen GJ. 2006. Magnetosomes are cell membrane imaginations organized by the actin-like protein MamK. Science 311:242–245.

Kostov I. 1968. Mineralogy Edinburgh, London: Oliver & Boyd. 580 p.

Li W, Yu L, Zhou P, Zhu M. 2007. A Magnetospirillum strain WM-1 from a freshwater sediment with intracellular magnetosomes. World J Microbiol Biotechnol 23:1489–1492.

Lins U, Farina M. 2004. Magnetosome chain arrangement and stability in magnetotactic cocci. Antonie van Leeuwenhoek, Intern J Gen Mol Microbiol 85:335–341.

Maier MR, Pepper I, Gerba C. 2009. Bacterial growth. In: Maier MR, Pepper I, Gerba C, editors. Environmental Microbiology. San Diego, CA: Academic Press. P 624.

Mann S, Sparks NHC, Frankel RB, Bazylinski DA, Jannasch HW. 1990. Biomineralization of ferrimagnetic greigite (Fe_3S_4) and iron pyrite (FeS_2) in a magnetotactic bacterium. Nature 343:258–261.

Martins JL, Silveira TS, Abreu F, Silva KT, Da Silva-Neto ID, Lins U. 2007. Grazing protozoa and magnetosome dissolution in magnetotactic bacteria. Environ Microbiol 9:2775–2781.

Matsunaga T, Sakaguchi T. 2000. Molecular mechanism of magnet formation in bacteria. J Biosci Bioeng 90:1–13.

Michaelis L, Menten ML. 1913. Kinetik der Invertinwirkung. Biochem Z 49:333–369.

Moisescu C, Bonneville S, Tobler D, Ardelean I, Benning LG. 2008. Controlled biomineralization of magnetite (Fe_3O_4) by *Magnetospirillum gryphiswaldense*. Mineral Mag 72:333–336.

Moskowitz BM. 1995. Biomineralization of magnetic minerals. Rev Geophys Suppl P 123–128.

Moskowitz BM, Bazylinski DA, Egli R, Frankel RB, Edwards KJ. 2008. Magnetic properties of marine magnetotactic bacteria in a seasonally stratified coastal pond (Salt Pond, MA, USA). Geophys J Inter 174:75–92.

Nakamura C, Burgess JG, Sode K, Matsunaga T. 1995. An iron-regulated gene, magA, encoding an iron transport protein of Magnetospirillum sp. strain AMB-1. J Biol Chem 270:28392–28396.

Okamura Y, Takeyama H, Matsunaga T. 2001. A Magnetosome-specific GTPase from the magnetic bacterium Magnetospirillum magneticum AMB-1. J Biol Chem 276:48183–48188.

Posfai M, Buseck PR, Bazylinski DA, Frankel RB. 1998. Iron sulfides from magnetotactic bacteria: Structure, composition, and phase transitions. Amer Mineral 83:1469–1481.

Scheffel A, Gruska M, Faivre D, Linaroudis A, Plitzko JM, Schüler D. 2006. An acidic protein aligns magnetosomes along a filamentous structure in magnetotactic bacteria. Nature 440:110–114.

Schleifer KH, Schüler D, Spring S, Weizenegger M, Amann R, Ludwig W, Köhler M. 1991. The genus *Magnetospirillum* gen. nov. Description of *Magnetospirillum gryphiswaldense* sp. nov. and transfer of *Aquaspirillum magnetotacticum* to *Magnetospirillum magnetotacticum* comb. nov. Syst Appl Microbiol 14:379–385.

Schubbe S, Kube M, Scheffel A, Wawer C, Heyen U, Meyerdierks A, Madkour MH, Mayer F, Reinhardt R, Schüler D. 2003. Characterization of a spontaneous nonmagnetic mutant of Magnetospirillum gryphiswaldense reveals a large deletion comprising a putative magnetosome island. J Bacteriol 185:5779–5790.

Schüler D. 1994. Isolierung und charakterisierung magnetischer bakterienuntersuchungen zur magnetitbiomineralisation in *Magnetospirillum gryphiswaldense*, PhD Thesis, Technische Universitat Munchen, Munich, Germany.

Schüler D. 1999. Formation of magnetosomes in magnetotactic bacteria. J Mol Microbiol Biotechnol 1:79–86.

Schüler D. 2002. The biomineralization of magnetosomes in Magnetospirillum gryphiswaldense. Intl Microbiol 5:209–214.

Schüler D, Baeuerlein E. 1996. Iron-limited growth and kinetics of iron uptake in Magnetospirillum gryphiswaldense. Arch Microbiol 166:301–307.

Schüler D, Baeuerlein E. 1997. Iron transport and magnetite crystal formation of the magnetic bacterium Magnetospirillum gryphiswaldense. J De Physique. IV: JP 7.

Schüler D, Baeuerlein E. 1998. Dynamics of iron uptake and Fe_3O_4 biomineralization during aerobic and microaerobic growth of Magnetospirillum gryphiswaldense. J Bacteriol 180:159–162.

Schüler D, Köhler M. 1992. The isolation of a new magnetic spirillum. Zentralbl Mikrobiol 147:150–151.

Simmons SL, Bazylinski DA, Edwards KJ. 2007. Population dynamics of marine magnetotactic bacteria in a meromictic salt pond described with qPCR. Environ Microbiol 9:2162–2174.

Simmons SL, Edwards KJ. 2006. The contribution of magnetotactic bacteria to reduced iron flux in stratified marine environments. Geochim Cosmochim Acta 70:A591–A591.

Simmons S, Edwards KJ. 2007. Geobiology of Magnetotactic Bacteria. In: Schüler D, editor. Magnetoreception and Magnetosomes in Bacteria. Microbial Monographs, Vol. 3. Heidelberg, Germany: Springer-Verlag. P 77–102.

Staniland S, Moisescu C, Benning LG. 2010. Cell division in magnetotactic bacteria splits magnetosome chain in half. J Basic Microbiol 50:1–5.

Stolz JF. 1992. Magnetotactic bacteria: biomineralization, ecology, sediment magnetism, environmental indicator. Catena Supplement 21:133–145.

Taylor AP, Barry JC. 2004. Magnetosomal matrix: Ultrafine structure may template biomineralization of magnetosomes. J Microsc 213:180–197.

Thomas-Keprta KL, Bazylinski DA, Kirschvink JL, Clemett SJ, McKay DS, Wentworth SJ, Vali H, Gibson Jr EK, Romanek CS. 2000. Elongated prismatic magnetite crystals in ALH84001 carbonate globules: Potential Martian magnetofossils. Geochim Cosmochim Acta 64:4049–4081.

Thomas-Keprta KL, Clemett SJ, Bazylinski DA, Kirschvink JL, McKay DS, Wentworth SJ, Vali H, Gibson Jr EK, McKay MF, Romanek CS. 2001. Truncated hexa-octahedral magnetite crystals in ALH84001: Presumptive biosignatures. Proc Natl Acad Sci USA 98:2164–2169.

Veblen DR, Post JE. 1983. A TEM study of fibrous cuprite (chalcotrichite); microstructures and growth mechanisms. Amer Mineral 68:790–803.

Widdel F, Bak F. 1992. Gram-negative mesophilic sulfate-reducing bacteria. In: Balows A, Trüper HG, Dworkin M, Harder W, Schleifer K-H (Eds.), The Prokaryotes, 2nd ed. New York: Springer-Verlag. P 3352–3378.

Winkelmann G. 1991. Specificity of iron transport in bacteria and fungi. In: Winkelmann G (ed.) editors. Handbook of Microbial Iron Chelates. Boca Raton, FL: CRC Press. P 65–106.

Xia M, Wei J, Lei Y, Ying L. 2007. A novel ferric reductase purified from Magnetospirillum gryphiswaldense MSR-1. Curr Microbiol 55:71–75.